ADVANCED MATERIALS
www.advmat.de

Doping Control via Molecularly Engineered Surface Ligand Coordination

*Mingjian Yuan, David Zhitomirsky, Valerio Adinolfi, Oleksandr Voznyy, Kyle W. Kemp, Zhijun Ning, Xinzheng Lan, Jixian Xu, Jin Young Kim, Haopeng Dong, and Edward H. Sargent**

Recent advances in materials processing has allowed for inexpensive and impressively efficient thin-film photovoltaic technologies based on inorganic solution-processed materials including CZTS[1–3] and the fast-advancing perovskites.[4–7] Colloidal quantum dots (CQDs)[8–13] are attractive materials for use in photovoltaic devices that, similarly, combine facile solution processing and low material cost, and add the benefit of quantum-size-effect dependent bandgap tunability. Size-tunability allows for tandem[11] and triple junction solar cells that are in principle capable of better harnessing the broad solar spectrum. Furthermore, being able to tune the same PbS CQD materials to be either n-type[27] and p-type has led to new CQD PV architectures[22] and potential application in novel electronic devices. Rapid progress in CQD photovoltaic device architectures and improvements in electronic material properties have led to certified AM 1.5 solar power conversion efficiencies of 7%.[14]

Novel device architectures have played a major role in the rapid improvement in power conversion efficiencies. Progress from the early Schottky structure[15] to the recent quantum junction[16,17] and multiple junction[11] architectures enabled increased efficiency of photogenerated charge extraction, raising device voltages, and offering a path towards further performance records. The best-performing devices to date have relied on the depleted-heterojunction architecture,[14] wherein a depleted p-type CQD solid forms the charge-separating heterojunction with an n-type TiO_2 or ZnO bulk transparent semiconductor.[18,19]

In the depleted-heterojunction structure, when a realistic load impedance for maximum power transfer is introduced, moving the device from short-circuit to maximum power point conditions, the device operating mode moves in the direction of forward bias. The depletion region then shrinks and a substantial quasi-neutral, undepleted, region emerges. This quasi-neutral region lacks a built-in electric field that would normally aid in the extraction of charge carriers.[20,21] Since, in CQD solids built to date, efficient harvesting of photocarriers relies on this built-in field, this increasing reliance on diffusion in the quasi-neutral region at high active layer thickness curtails the performance of the solar cell, reducing its fill factor.

An improved device architecture has recently been proposed that seeks to overcome this limitation of the depleted heterojunction approach. In the graded doping approach,[22] a spatial gradient in the doping within a light-absorbing type CQD solid allowed more efficient extraction of carriers at the maximum power point, and also increased the built-in potential and thus the voltage. Building such a gradient relied on the availability of CQD solid materials having a wide and well-controlled range of dopings.

The graded doping strategy was recently implemented on the n-side of a quantum junction solar cell.[22] It would be particularly attractive to implement it in the best-performing depleted heterojunction architecture; however, control of doping of a high-photovoltaic-performance p-type CQD solid has not previously been reported.

We took the view that tuning the chemistry at the CQD surface could offer an avenue to controllable p-type doping.[23,29,30] Synthetic and postsynthetic chemical treatments allow, in principle, control over the free carrier concentrations in quantum dot solids.[25] Control over doping type in CQDs films has been demonstrated via electrochemistry,[24] judicious choice of ligands,[26] exposure to atmospheric oxygen,[16,27] and post-treatment with selected cations or anions.[28] In general, the net doping is determined by the overall stoichiometry, that is to say the balance between the cationic and anionic species, taking into account both inorganic atoms and also molecular ligands.[29,30]

PbS CQD films exhibit an excess of lead atoms because their synthesis relies on ligands that bind only to cations, thus favoring Pb-terminated surfaces. From stoichiometric considerations, the inorganic core of these CQDs, i.e., ignoring their ligands, is expected to be strongly n-type (**Figure 1**a).[27,29] This Pb excess is offset by surface ligands and oxygen, which can accept excess electrons from the conduction band (Figure 1b) and eventually from the valence band itself, resulting in a p-type PbS CQD solid (Figure 1c). During the preparation of a CQD solid, native oleic acid ligands are replaced by shorter thiol-based ligands, and the surface can react with atmospheric oxygen if present. Typically, short cross-linking ligands such as ethane dithiol (EDT)[31] or 3-mercaptopropionic acid (MPA) are employed.[32]

To achieve a net doping level closer to intrinsic, the extent of introduction of p-doping agents (ligands and oxygen) can be reduced. Processing in a nitrogen glovebox atmosphere has been shown to reduce p-doping.[27] However, to build a

Dr. M. Yuan,[+] D. Zhitomirsky,[+] V. Adinolfi, Dr. O. Voznyy, K. W. Kemp, Dr. Z. Ning, X. Lan, J. Xu, Dr. J. Y. Kim, H. Dong, Prof. E. H. Sargent
Department of Electrical and Computer Engineering
University of Toronto
10 King's College Road, Toronto, Ontario, M5S 3G4, Canada
E-mail: ted.sargent@utoronto.ca
[+]M.Y. and D.Z. contributed equally to this work.

DOI: 10.1002/adma201302802

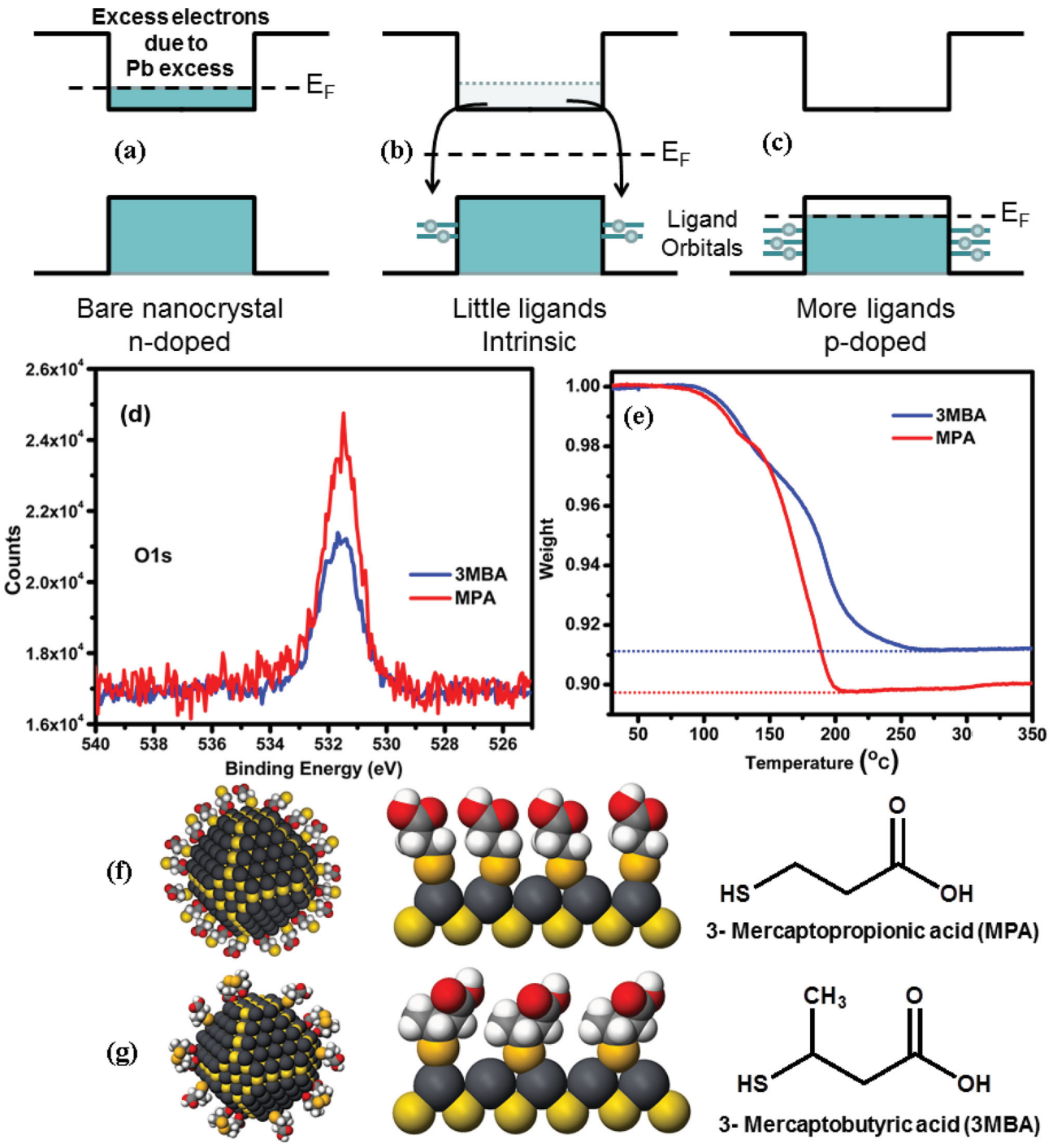

Figure 1. Doping via control over ligand coverage. (a) n-doping due to a lead excess, leading the Fermi level to reside near the conduction band edge; (b) shift of the Fermi level to the mid-gap due to an increased quantity of surface ligands; (c) further shift towards the valence band giving rise to free holes due to additional anionic ligands. (d) XPS data showing different amount of oxygen (corresponding to carboxyl group) for films exchanged to MPA and 3MBA ligands, indicating a greater molecular abundance of MPA; (e) Thermogravimetric analysis data for MPA and 3MBA ligands treated CQD solid, indicating a greater molecular coverage of MPA; (f) and (g) posited packing density due to steric limits of MPA and 3MBA, respectively, showing reduced packing for 3MBA. The black dot represents lead atoms, yellow dot represents sulfur atoms and the red dot represent oxygen atoms.

quantum dot solid having graded doping, processing within a single atmosphere is desirable, as any attempts to make a more intrinsic material in an inert atmosphere may be negated by subsequent re-exposure to air ambient. We therefore desired a means of controlling doping that would be implemented and preserved across a complex materials stack.

We posited that we could use the structure of "designer" bidentate ligands to lower, in a controlled fashion, the density of

Adv. Mater. **2013**,
DOI: 10.1002/adma201302802

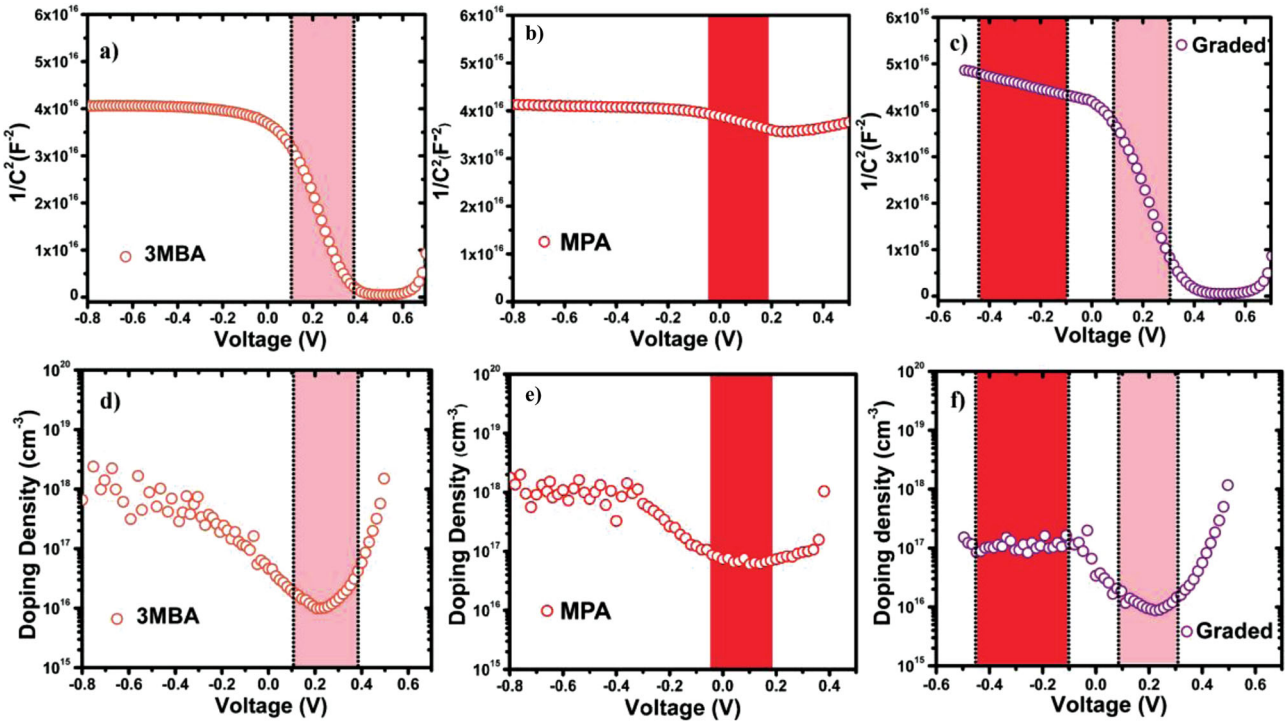

Figure 2. Experimental analysis of doping in various liganded CQD solids. Capacitance-voltage studies for (a) 3MBA, (b) MPA and the (c) graded architecture. In (d), (e) and (f), Mott-Schottky analysis is presented for the corresponding samples. In (a)-(c) the linear region corresponding to the change in the depletion width with voltage is highlighted in each case. The corresponding doping density is calculated over this range and is shown in (d)-(f). The plateau in each curve represents the doping density for the respective material. In (f) two such plateaus are evident, corresponding to the doping densities of the p+ and p-type layers making up the graded device.

ligands on surface, thereby allowing us to tune the hole density in the film. To maintain a consistent degree of protection from the oxidizing atmosphere, such a ligand would need to be bulky. Recently, 3-mercaptobutyric acid (3MBA) has been reported to improve the air stability and PLQY of CdTe CQDs.[33] 3MBA has the same functional groups as MPA, but consists of a branched carbon chain, with an extra methyl group close to thiol group (Figure 1g). XPS reveals that (Figure 1d) the amount of oxygen related to carboxyl groups is much greater in MPA-treated than in the 3MBA-treated films (O_MPA 0.49±0.06, O_3MBA 0.38 ± 0.07). The Pb-S stoichiometry and the quantity of halides remained unchanged for the two treatments (Figure S15-S18).

We carried out thermogravimetric analysis (TGA) for both MPA- and 3MBA-treated CQD solids to further challenge our hypothesis. It revealed (Figure 1e) a 9 ± 0.4% weight loss for 3MBA-treated CQD solids, lower than 10.2 ± 0.2% weight loss for the MPA-treated case. Since 3MBA has higher molecular weight than MPA, the surface coverage of 3MBA is thus considerably lower. Together with XPS, this suggests that due to steric interactions, it is possible to incorporate more MPA ligands than 3MBA on the CQD surface. Furthermore, TGA-Mass Spectrometry probing the loss of each ligand confirmed that more ligands were present in MPA films compared to films made with 3MBA (Figures S4–S10).

These findings confirm the hypothesis that we can regulate the coverage of the CQD surface via steric interactions. According to the stoichiometry, or charge-balance, model of CQD doping,[29] the resultant lower incorporation of anionic ligands should lead to a decreased doping density, a possibility we were able to investigate using capacitance-voltage measurements and subsequent Mott-Schottky analysis.[30,34]

Capacitance-voltage measurements were carried out on depleted heterojunction devices employing p-type CQD active layers made using each of the ligands under investigation. **Figures 2**a and b show the experimental $1/C^2$ obtained for these 3MBA and MPA ungraded devices, respectively. In Figures 2 (d) and (e) we obtain the doping density via Mott-Schottky analysis, focusing on the highlighted regions in which the capacitance is changing linearly with voltage.

At higher voltages, each device is largely undepleted; while at lower voltage, it approaches full depletion. The analysis shows that 3MBA has a doping density of 8×10^{15} ($\pm 1 \times 10^{15}$) cm^{-3}, while the MPA device exhibits 6×10^{16} ($\pm 1 \times 10^{16}$) cm^{-3} net doping. Thus, adopting and deploying the stoichiometric and steric hindrance picture of doping enabled an order-of-magnitude control over net doping.

We therefore proceeded to investigate photovoltaic devices employing graded doping[22] based on the molecularly-engineered surface ligand coordination strategy. Our goal was to build a device having an active p-type CQD absorber whose doping was lower near the interface with the TiO_2 interface, and increased approaching the Ohmic contact to the p-side.

To implement and validate true spatially-graded doping, we would need first to establish that the doping densities would be retained when these materials were combined into a single device. To address this point, we built depleted heterojunction

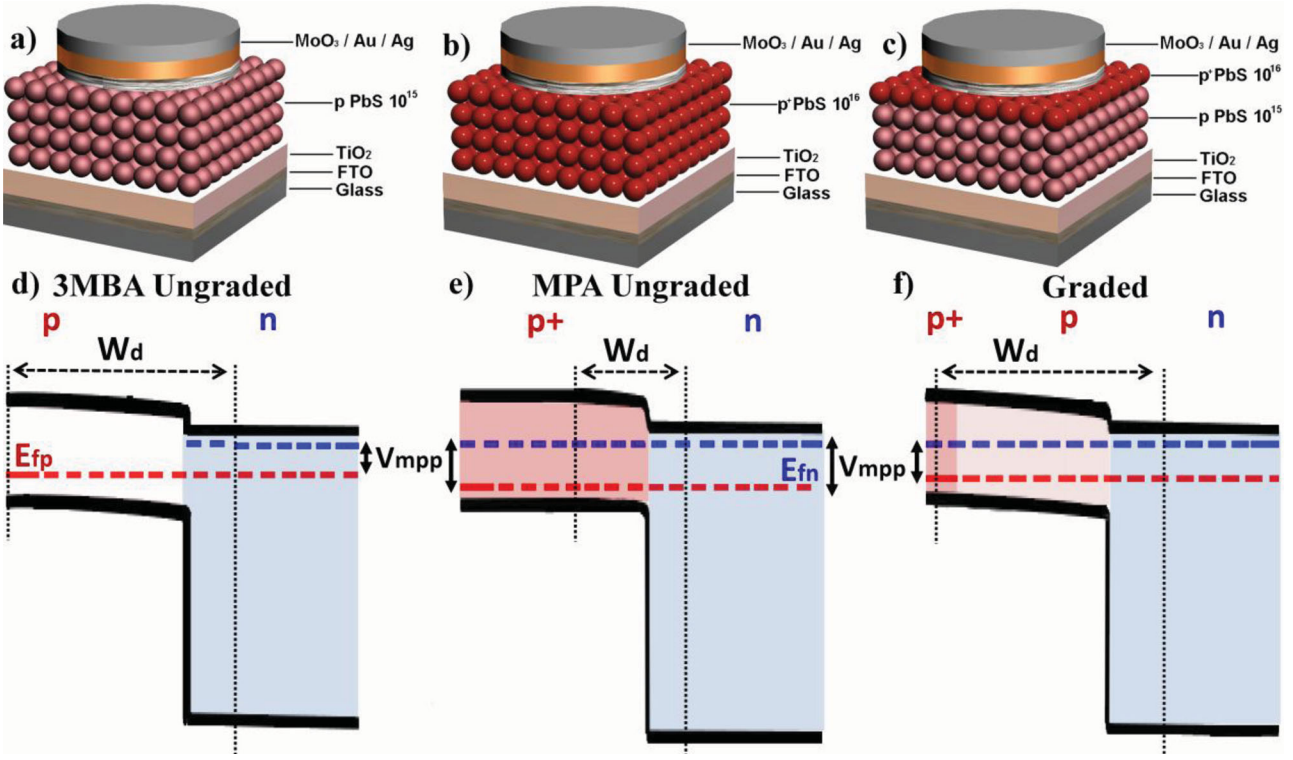

Figure 3. Architecture of control and graded-doping devices. (a)-(c) present the 3MBA, MPA, and graded device architectures, respectively. (d)-(f) present the corresponding spatial band diagrams simulated at the maximum power point under AM 1.5 solar illumination. In d) The low doping density of the p-layer provides a wide depletion region from which charge carriers are efficiently extracted, but a low voltage due to the low built-in potential. In contrast, the device in (e) employs the highly doped p+ layer and shows a high voltage; but its thinner depletion region degrades photocurrent. In (f), the graded structure properly combines a p+ followed by a p-type layer to achieve high current, owing to its wide depletion region, and an increased voltage compared to the device in (d) as a result of higher splitting of the quasi Fermi energies provided by the p+ layer.

devices in which the first 280 nm consisted of PbS CQDs treated with 3MBA, while the remaining 90 nm employed the higher doped MPA treated PbS CQDs, as would be required for a graded doping device. Capacitance-voltage results are shown in Figures 2c. Mott-Schottky analysis (Figures 2f) confirms that two doping plateaus are present in our device [$8 \times 10^{15}(\pm 0.5 \times 10^{15})$ and $8 \times 10^{16}(\pm 1 \times 10^{16})$] cm^{-3}, in good agreement with the doping densities measured for these materials separately. Reproducibility was verified by doing multiple trials for each class of materials (Figures S12-S14).

We now evaluate the performance of the uniformly-doped control devices compared to the graded device, first using modeling, and then using experiment. **Figures 3**a-c show device stacks for the 3MBA, MPA, and graded device architectures, respectively. The 3MBA PbS CQD material is designated as p-PbS, while the higher doped MPA-treated CQDs are designated as p^+-PbS. To achieve the best device performance, the p+ layer is chosen to be thinner than the p layer, as has been previously shown for the n-type materials,[22] and depicted in Figure 3c. The incorporation of a high work-function hole collecting MoO_3 layer provided an Ohmic contact to the PbS layer.[39,41] We simulate the expected spatial band diagrams of these devices using SCAPS[35,36] at the maximum power point to validate the origin of the expected enhancement. To verify whether the position of the bands shifted as a result of the different surface treatments,[10,38] we carried out cyclic voltammetry experiments that showed fixed band positions within experimental uncertainty (Figure S2). Figure 3d shows the 3MBA device at the maximum power point, still largely depleted due to its reduced doping. This structure allows good current extraction, but the lower doping limits Fermi-level splitting required for a high voltage, as evidenced when compared with Figure 3e, where the MPA device has greater Fermi level separation. The graded structure (Figure 3f) exhibits good depletion and good Fermi level separation, owing to the newly introduced grading scheme. In effect, the p^+ layer is able to aid in more efficiently depleting the p layer by introducing an electric field at the p/p^+ junction, while maintaining good Fermi separation at the contact.

We then characterized, as photovoltaic devices, experimental instantiations of the three class of devices explored above. **Figure 4**a,b shows the dark and light J-Vs of all three classes of devices. The diode turn-on voltage behavior and reverse saturation currents (Figure S3) of the dark J-V curves show that the doping difference in the different p-type CQD solids accounts for the differing built-in voltages, offering an explanation for the voltages observed at open circuit in the light J-V curves.[22] The standard solar cell performance metrics are summarized in Figure 4c, and EQE spectra are provided for each class of device (Figure S20). The graded device outperforms both the MPA and 3MBA devices in terms of short circuit current (J_{SC}) and has an open circuit voltage (V_{OC}) intermediate between the MPA and 3MBA devices. The device's fill factor, the measure of

Adv. Mater. **2013**,
DOI: 10.1002/adma201302802

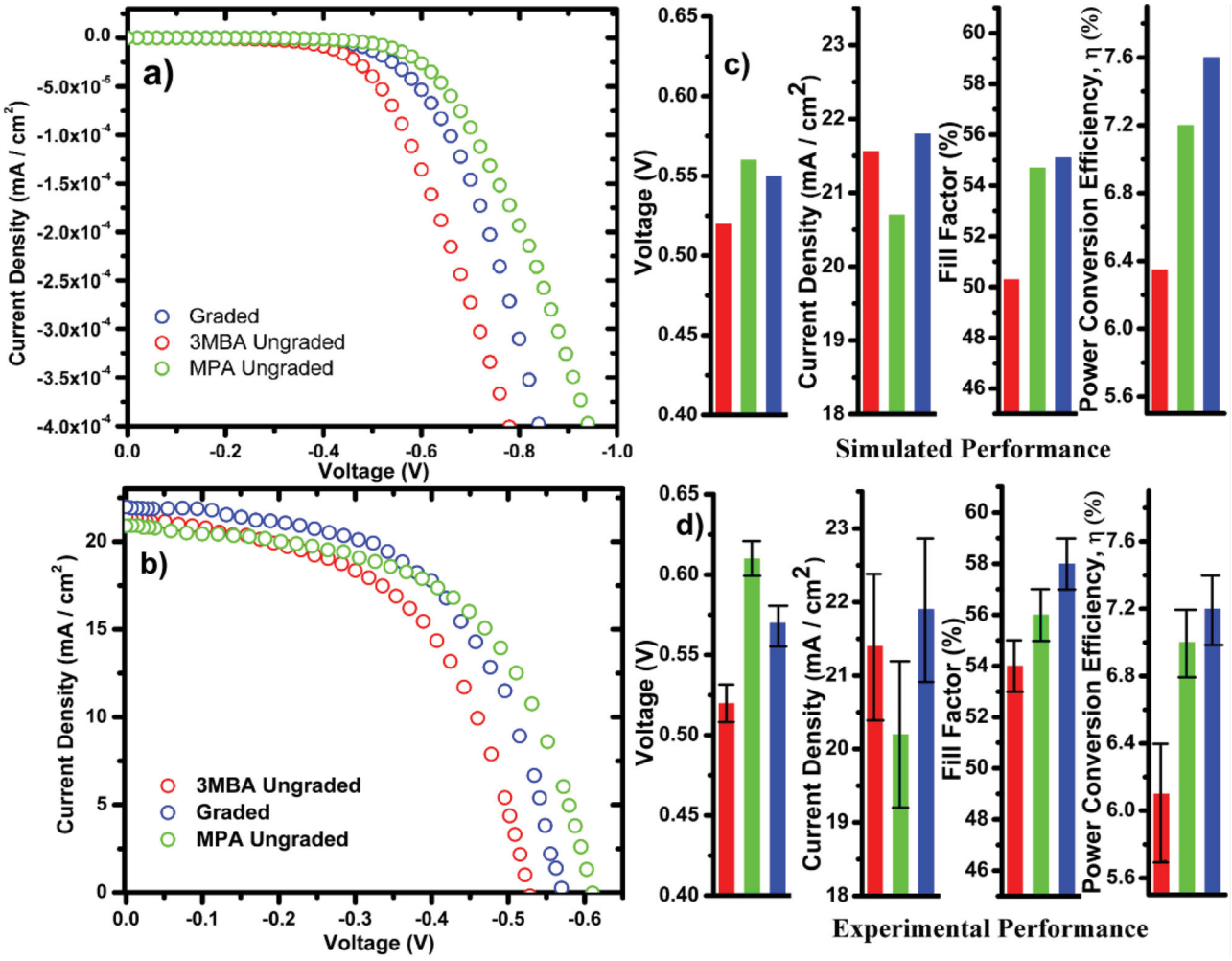

Figure 4. Performance of control and graded-doping devices. (a) Experimental Dark J-V and (b) light J-V curves for 3MBA, MPA and graded devices. (c) simulated performance metrics of each device using realistic device parameters and (d) experimental performance metrics for the each class of device.

the device's ability to maintain its J_{SC} and V_{OC} at its maximum power point, is highest in the graded device, as expected from considerations from the simulated band diagrams in Figure 3. This leads to an overall best efficiency of 7.2 ± 0.2% (Table S1) for the graded device. In order to study the impact of the grading further, we verified the operation of a device graded in the opposite direction (with the p and p^+ layer reversed). Such a device would be expected to drive minority carriers in the undesired direction, as observed experimentally in its low measured current and fill factor (Figure S9). Finally, Figures 4d show simulated performance metrics based on test structures employing the parameters of each device. The model and experiment are in excellent agreement, highlighting the improved performance attained using the graded structure.

In conclusion, we identified a means to control the net doping of a CQD solid via the design of the bidentate ligand crosslinking the material. The strategy does not rely on implementing different atmospheres at different steps in device processing, but instead is a robust strategy implemented in a single processing ambient. We achieve an order of magnitude difference in doping that allows us to build a graded photovoltaic device and maintain high current and voltage at maximum power-point conditions. This work points to further avenues to exploit controlled spatial doping profiles in CQD optoelectronics.

Experimental Section

Synthesis of 3-Mercaptobutyric Acid: To a 50 mL flask was introduced crotonic acid (8.4 g, 100 mmol) and thioacetic acid (8.36 g, 110 mmol). The resulting mixture was stirred for 24 h at room temperature, then heated up to 50 °C for 6 h. The obtained 3-acetylmercaptobutyric acid was treated with 100 mL of concentrated NaOH solution for 2 h. Then, the resulting solution was acidified with 100 mL of H_2SO_4 and extracted with diethyl ether for two times. The organic phase was dried over anhydrous Na_2SO_4, the solvent was removed under reduced pressure, and the residue was purified by distillation, 7.6 g of pure 3-Mercaptobutyric acid (3MBA) was finally obtained as yellowish liquid. (Yield, 63%). ^{1}H NMR (300 MHz, $CDCl_3$): 1.43 (d, 3H), 1.91(d, 1H), 2.52 (m, 3H), 3.34 (m, 1H), 10.42 (b, 1H). GC-MS: ($C_4H_8O_2S$) 120.17, found 121.1. Elemental analysis performed for $C_4H_8O_2S$ (%), C: 39.98, H:6.71. S:26.68 and for $C_4H_8O_2S$ (%), C: 39.73, H:6.84, S 26.92.

Quantum Dot Synthesis: PbS quantum dots were synthesized according to a previously published method.[37] The PbS quantum dots used in this study were applied for metal halide ($CdCl_2$) treatment

according to the reference.[14] The bandgap for the PbS quantum dots used in this study is 1.3 eV.[14]

Photovoltaic Device Fabrication: PbS CQD films were deposited using a layer-by-layer spin-casting process. For each layer, the PbS CQD in Octane (50 mg/mL) were deposited on the TiO_2/FTO substrate[42] and spin-cast at 2500 rpm for 10 seconds. Solid state ligand exchange process is similar to the previous report.[14] In the ungraded architecture, for the p-PbS layers, a methanol solution containing 1% 3MBA (V/V) was dispensed to the substrate and spun after 3 seconds at the same speed for 5 seconds. Two times methanol washing was applied to remove unbounded ligands. For the p^+-PbS layers, the 1% MPA: methanol (V/V) was used for the solid-state ligand exchange process with the same procedure.

In the graded architecture, first nine layers were constructed by 1% 3MBA methanol solution (V/V) treated dots following above procedure (p-PbS layers), then 1% MPA treated dots were used for last three layers (p^+-PbS layers) in order to reach the final thickness.

In the anti-graded architecture (Figure S21), first nine layers were constructed by 1% MPA methanol solution (V/V) treated dots (p^+-PbS layers) following above procedure, then 1% 3MBA treated dots were used for last three layers (p-PbS layers) in order to reach the final thickness.

The film thickness was measured through a DekTak 3 Profilometer, the average film thickness for 12 LBL MPA ungraded, 3MBA ungraded and Graded device is 370 ± 10 nm (Figure S24).

Top electrodes were deposited using an Angstrom Engineering deposition system in an Innovative Technology glovebox. The contacts typically consisted of 7.5 nm thermally evaporated molybdenum trioxide deposited at a rate of 0.2 Å S^{-1}, followed by electron-beam deposition of 50 nm of gold deposited at 0.4 Å S^{-1}, and finally 120 nm of thermally evaporated silver deposited at 1.0 Å S^{-1}.

Photovoltaic performance characterization: Current-voltage characteristics were measured using a Keithley 2400 source-meter in N_2 ambient. The solar spectrum at AM1.5 was simulated to within class A specifications (less than 25% spectral mismatch) with a Xe lamp and filters (Solar Light Company Inc.) with measured intensity at 100 mW cm^{-2}. The source intensity was measured using a Melles-Griot broadband power meter and a Thorlabs broadband power meter through a circular 0.049 cm^2 aperture at the position of the device and confirmed with a calibrated reference solar cell (Newport, Inc.). The spectral mismatch of the system was characterized using a calibrated reference solar cell (Newport). The total AM 1.5 spectral mismatch taking into account the simulator spectrum and the spectral responsivities of the test cell, reference cell, and broadband powermeter was re-measured periodically and found to be 5%. This multiplicative factor, M = 0.95, was applied to the current density values of the J–V curve to most closely resemble true AM 1.5 performance.

XPS measurement: The surface elements and chemical states of PbS CQDs were examined using X-ray photoelectron spectroscopy (XPS) (PHI-5500) with a monochromated Al K radiation source (1486.7 eV) to excite photoelectrons in an ultrahigh vacuum atmosphere at ≈10^{-9} Torr. The binding-energy scale was calibrated using the Au 4f 7/2 peak to 83.98 eV and the Cu 2p 3/2 peak of sputter-cleaned Cu to 932.67 eV.

Capacitance-Voltage measurement: ZnO[14,40] was used as the complementary electrode to form the rectifying junction with PbS. Capacitance-voltage (C-V) measurements were performed using an Agilent 4284A precision LCR meter under Cp-Rp model. All measurements were performed in the dark. CV sweeps of solar cell devices were performed between –1 and +1 V with an AC signal of 10 mV and 1000 Hz.

Optoelectronic Simulation: SCAPS 3.0.01[35,36] was used for the optoelectronic simulations. Details of the simulations are found in the Supporting Information (Table S1-S3).

Supporting Information

Supporting Information is available from the Wiley Online Library or from the author.

Acknowledgements

This publication is based in part on work supported by Award KUS-11–009–21, made by King Abdullah University of Science and Technology (KAUST), by the Ontario Research Fund Research Excellence Program, and by the Natural Sciences and Engineering Research Council (NSERC) of Canada. D. Zhitomirsky acknowledges the financial support through the NSERC CGS D Scholarship. We thank Angstrom Engineering and Innovative Technology for useful discussions regarding material deposition methods and control of glovebox environment, respectively. The authors would like to acknowledge the technical assistance and scientific guidance of E. Palmiano, R. Wolowiec, and D. Kopilovic.

Received: June 18, 2013
Published online:

[1] Q. Guo, G. M. Ford, W.-C. Yang, B. C. Walker, E. A. Stach, H. W. Hillhouse, R. Agrawal, *J. Am. Chem. Soc.* **2010**, *132*, 17384.
[2] T. K. Todorov, J. Tang, S. Bag, O. Gunawan, T. Gokmen, Y. Zhu, D. B. Mitzi, *Adv. Energy. Mater.* **2013**, *3*, 34.
[3] T. K. Todorov, K. B. Reuter, D. B. Mitzi, *Adv. Mater.* **2010**, *22*, E156.
[4] M. M. Lee, J. Teuscher, T. Miyasaka, T. N. Murakami, H. J. Snaith, *Science*, **2012**, *338*, 634.
[5] J. H. Heo, S. H. Im, J. H. Noh, T. N. Mandal, C.-S. Lim, J. A. Chang, Y. H. Lee, H.-J. Kim, A. Sarkar, M. K. Nazeeruddin, M. Gratzel, S. II. Seok, *Nature Photon.* **2013**, *7*, 486.
[6] L. Etgar, P. Gao, Z. Xue, Q. Peng, A. K. Chandiran, B. Liu, M. K. Nazeeruddin, M. Gratzel, *J. Am. Chem. Soc.* **2012**, *134*, 17396.
[7] J. M. Ball, M. M. Lee, A. Hey, H. Snaith, *Energy Environ. Sci.* **2013**, *6*, 1739.
[8] M. Grätzel, R. A. J. Janssen, D. B. Mitzi, E. H. Sargent, *Nature* **2012**, *488*, 304.
[9] O. E. Semonin, J. M. Luther, S. Choi, H.-Y. Chem, J. Gao, A. J. Nozik, M. Beard, *Science.* **2011**, *334*, 1530.
[10] J. Tang, K. W. Kemp, S. Hoogland, K. S. Jeong, H. Liu, L. Levinal, M. Furukawa, X. Wang, R. Debnath, D. Cha, K. Chous, A. Fischer, A. Amassians, J. B. Asbury, E. H. Sargent, *Nature Mater.* **2011**, *10*, 765.
[11] X. Wang, G. I. Koleilat, J. Tang, H. Liu, I. J. Kramer, R. Debnath, L. Brzozowski, D. A. R. Barkhouse, L. Levina, S. Hoogland, E. H. Sargent, *Nature Photon.* **2011**, *5*, 480.
[12] D. V. Talapin, J. S. Lee, M. V. Kovalenko, E. V. Shevchenko, *Chem. Rev.* **2010**, *110*, 389.
[13] A. Nozik, M. Beard, J. Luther, M. Law, R. Ellingson, J. Johnson, *Chem. Rev.* **2010**, *110*, 6873.
[14] A. H. Ip, S. M. Thon, S. Hoogland, O. Voznyy, D. Zhitomirsky, R. Debnath, L. Levina, L. R. Rollny, G. H. Carey, A. Fischer, K. W. Kemp, I. J. Kramer, Z. Ning, A. J. Labelle, K. W. Chou, A. Amassian, E. H. Sargent, *Nature Nanotech.* **2012**, *7*, 577.
[15] K. W. Johnsto, A. G. Pattantyus-Abraham, J. P. Clifford, S. H. Myrskog, D. D. MacNeil, L. Levina, E. H. Sargent, *Appl. Phys. Lett.* **2008**, *92*, 151115.
[16] J. Tang, H. Liu, D. Zhitomirsky, S. Hoogland, X. Wang, M. Furukawa, L. Levina, E. H. Sargent, *Nano Lett.* **2012**, *12*, 4889.
[17] A. K. Rath, M. Bernechea, L. Martinez, F. P. G. de Arquer, J. Osmond, G. Konstantatos, *Nature Photon.* **2012**, *6*, 529.
[18] A. G. Pattantyus-Abraham, I. J. Kramer, A. R. Barkhouse, X. Wang, G. Konstantatos, R. Debnath, L. Levina, I. Raabe, M. K. Nazeeruddin, M. Gratzel, E. H. Sargent, *ACS Nano.* **2010**, *4*, 3374.
[19] J. Gao, J. M. Luther, O. E. Semonin, J. Randy, A. J. Nozik, M. C. Beard, *Nano Lett.* **2011**, *11*, 1002.
[20] K. W. Johnston, A. G. Pattantyus-Abraham, J. P. Clifford, S. H. Myrskog, S. Hoogland, H. Shukla, E. J. D. Klem, L. Levina, E. H. Sargent, *Appl. Phys. Lett.* **2008**, *92*, 122111.

[21] J. T. Stewart, L. A. Padilha, M. Q. Qazilbash, J. M. Pietryga, A. G. Midgett, J. M. Luther, M. C. Beard, A. J. Nozik, V. I. Klimov, *Nano Lett.* **2012**, *12*, 622.
[22] Z. Ning, D. Zhitomirsky, V. Adinolfi, B. Sutherland, J. Xu, O. Voznyy, P. Maraghechi, X. Lan, S. Hoogland, Y. Ren, E. H. Sargent, *Adv. Mater.* **2013**, *25*, 1719.
[23] T. P. Osedach, N. Zhao, T. L. Andrew, P. R. Brown, D. D. Wanger, D. B. Strasfeld, L.-Y. Chang, M. G. Bawendi, V. Bulovic, *ACS Nano.* **2012**, *6*, 3121.
[24] J. H. Engel, Y. Surendranath, A. P. Alivisatos, *J. Am. Chem. Soc.* **2012**, *134*, 13200.
[25] A. Sahu, M. S. Kang, A. Kompch, C. Notthoff, A. W. Wills, D. Deng, M. Winteter, C. D. Frisbie, D. J. Norris, *Nano Lett.* **2012**, *12*, 2587.
[26] D. V. Talapin, C. B. Murray, *Science* **2005**, *310*, 86.
[27] D. Zhitomirsky, M. Furukawa, J. Tang, P. Stadler, S. Hoogland, O. Voznyy, H. Liu, E. H. Sargent, *Adv. Mater.* **2012**, *24*, 6181.
[28] A. Nag, D. S. Chung, D. S. Dolzhnikov, N. M. Dimitrijevic, S. Chattopadhyay, T. Shibata, D. V. Talapin, *J. Am. Chem. Soc.* **2012**, *134*, 13604.
[29] O. Voznyy, D. Zhitomirsky, P. Stadler, Z. Ning, S. Hoogland, E. H. Sargent, *ACS Nano.* **2012**, *6*, 8448.
[30] S. J. Oh, N. E. Berry, J. Choi, E. A. Gaulding, T. Paik, S. Hong, C. B. Murry, C. R. Kagan, *ACS Nano.* **2013**, *7*, 2413.
[31] P. R. Brown, R. R. Lunt, N. Zhao, T. P. Osedach, D. D. Wanger, L. Chang, M. G. Bawendi, V. Bulovic, *Nano Lett.* **2011**, *11*, 2955.
[32] K. S. Jeong, J. Tang, H. Liu, J. Kim, A. W. Schaefer, K. Kemp, L. Levina, X. Wang, S. Hoogland, R. Debnath, L. Brzozowski, E. H. Sargent, J. B. Asbury, *ACS Nano.* **2012**, *6*, 89.
[33] T. Fang, K. Ma, L. Ma, J. Bai, X. Li, H. Song, H. Guo, *J. Phys. Chem. C.* **2012**, *116*, 12346.
[34] F. Recart, A. Cuevas, *Electron Devices, IEEE Transactions on.* **2006**, *53*, 442.
[35] M. Burgelman, P. Nollet, S. Degrave, *Thin Solid Films.* **2000**, *361–362*, 527.
[36] M. Burgelman, J. Verschraegen, S. Degrave, P. Nollet, *Prog. Photovolt: Res. Appl.* **2004**, *12*, 143.
[37] M. A. Hines, G. D. Scholes, *Adv. Mater.* **2003**, *15*, 1844.
[38] R. R. Gagne, C. A. Koval, G. C. Lisensky, *Inorg. Chem.* **1980**, *19*, 2854.
[39] P. R. Brown, R. R. Lunt, N. Zhao, T. P. Osedach, D. D. Wanger, L.-Y. Chang, M. G. Bawendi, V. Bulovic, *Nano Lett.* **2011**, *11*, 2955.
[40] K. W. Kemp, A. J. Labelle, S. M. Thon, A. H. Ip, I. J. Kramer, S. Hoogland, E. H. Sargent, *Adv. Energy. Mater.* **2013**, DOI: 10.1002/aenm.201201083.
[41] X. Wang, G. I. Koleilat, A. Fischer, J. Tang, R. Debnath, L. Levina, E. H. Sargent, *ACS. Appl. Mater. Interfaces.* **2011**, *3*, 3792.
[42] H. Liu, J. Tang, I. J. Kramer, R. Debnath, G. I. Koleilat, X. Wang, A. Fisher, R. Li, L. Brzozowski, L. Levina, E. H. Sargent, *Adv. Mater.* **2011**, *23*, 3832.